Journal of Materials Chemistry C

ROYAL SOCIETY OF CHEMISTRY

PAPER

View Article Online
View Journal | View Issue

Check for updates

Cite this: J. Mater. Chem. C, 2021, 9, 6470

Disilane-bridged architectures with high optical transparency for optical limiting†

Hongjie Feng,[a] Zhikuan Zhou, *[a] Aviwe K. May,[b] Jiaying Chen,[a] John Mack, *[b] Tebello Nyokong,[b] Lizhi Gai[a] and Hua Lu *[a]

Received 31st March 2021,
Accepted 27th April 2021

DOI: 10.1039/d1tc01488a

rsc.li/materials-c

A novel tetraphenylethylene (TPE) architecture that makes use of a disilane bridge was developed to successfully prepare organic optical power limiting (OPL) materials with high transparency. The σ-bridged TPE derivatives exhibit enhanced solid-state emission efficacies up to 4 times that of TPE. Due to the unique σ-electron delocalization, the incorporated Si–Si bridge gives rise to intense nonlinear optics (NLO) properties. These compounds show favorable optical transparency in the visible region, since the σ–π interaction has a relatively minor effect on the absorption properties of TPE. The poly(bisphenol A carbonate) (PBC) thin films of disilane-bridged compounds exhibit significant reverse saturable absorbance (RSA) responses during Z-scan measurements at 532 nm. In contrast, negligible OPL properties were observed in tetrahydrofuran (THF) solution and when a PBC thin film was prepared with TPE. The disilane-bridged molecular system represents a novel and easily prepared architecture for the construction of solid-state optical limiting materials.

Published on 28 April 2021. Downloaded by Rhodes University on 11/3/2021 3:22:14 PM.

Introduction

Optical power limiting (OPL) is an ideal mechanism for protection from high-intensity laser exposure and is one of the major research areas of interest in nonlinear optics (NLO).[1] Molecules and materials suitable for OPL must possess high transmittance of low-intensity light, along with the ability to attenuate an intense optical beam, thus limiting the output fluence.[2] The most promising strategy in limiting nanosecond (ns) or picosecond (ps) laser pulses is the use of NLO materials that exhibit either intense nonlinear absorption or nonlinear scattering responses.[3] Organic π-conjugated molecules, such as fullerenes,[4] BODIPYs,[5] porphyrins,[6] phthalocyanines,[7] and D–π–A motifs,[8] are commonly studied for OPL applications because of their high degree of structural flexibility and processability, optimal band gaps, and high optical susceptibilities.[9] However, most of these molecules exhibit limited transparency in the visible region due to the large numbers of delocalized π-electrons or the presence of a π–π* intramolecular charge transfer (ICT) transitions that generate NLO properties.[10] Although elegant molecular engineering has been carried out to decrease or minimize the extent of π-conjugation to eliminate opacity in the visible region, these molecules usually exhibit OPL properties in solution,[11] which is not favorable in practice. Consequently, the search for novel compounds with enhanced transparency along with strong nonlinear responses in the solid state remains the main challenge for various applications in the OPL field.

Recently, σ–π conjugated molecular systems with saturated Si–Si σ bonds inserted between two π-systems have attracted considerable interest because they exhibit enhanced photoluminescence (PL)[12] and electron-transporting properties,[13] NLO responses and multifunctional behavior.[14] Organosilicon compounds exhibit significant NLO responses due to increased polarizability of the Si backbone, p–d orbital bonding, and σ–π interactions.[14b,15] We propose that the introduction of a Si–Si σ-bond into small organic molecules such as tetraphenylethylene (TPE) derivatives[16] would produce materials with a favorable "trade-off" between transparency and OPL properties in the solid state (Scheme 1). In this study, we explore whether σ-bridged TPE dyes retain the original absorption and emission color of TPE but with significantly enhanced solid-state emission, and whether the photophysical properties can be fine-tuned by adjusting the end-capped substituents with donor and acceptor properties to form TPE–Si–Si-D and TPE–Si–Si-A dyes, respectively.

Herein, we report a series of novel σ-bridged molecules with permethylated disilane as linkers (Scheme 2). The linear optical properties both in solution and the solid state were investigated. Their favorable transparency in the visible region

[a] Key Laboratory of Organosilicon Chemistry and Material Technology of Ministry of Education, and Key Laboratory of Organosilicon Material of Zhejiang Province, Hangzhou Normal University, No. 2318, Yuhangtang Road, Hangzhou 311121, P. R. China. E-mail: zkzhou@hznu.edu.cn, hualu@hznu.edu.cn

[b] Institute for Nanotechnology Innovation, Department of Chemistry, Rhodes University, Makhanda 6140, South Africa. E-mail: j.mack@ru.ac.za

† Electronic supplementary information (ESI) available. CCDC 2061563 and 2061564. For ESI and crystallographic data in CIF or other electronic format see DOI: 10.1039/d1tc01488a

This journal is © The Royal Society of Chemistry 2021

Published on 28 April 2021. Downloaded by Rhodes University on 11/3/2021 3:22:14 PM.

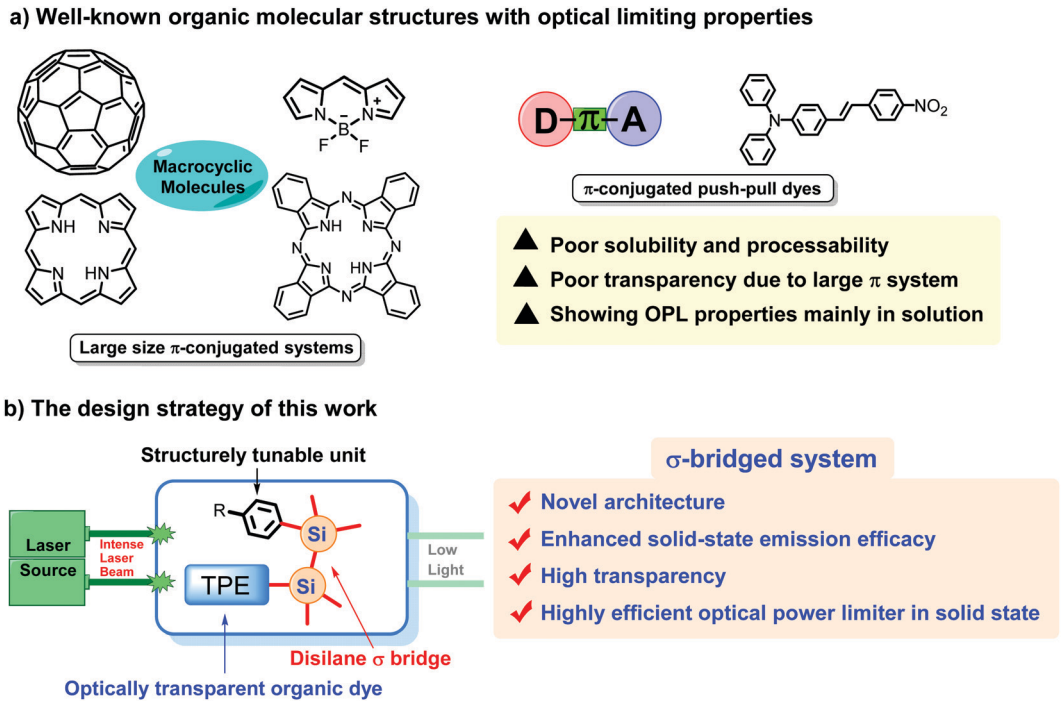

Scheme 1 (a) The molecular structures of representative organic OPL materials and (b) the molecular design of this work.

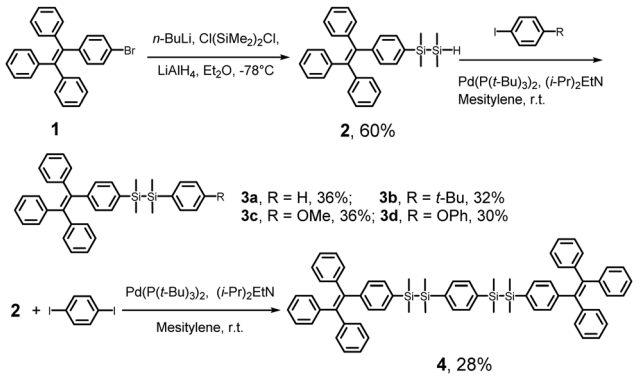

Scheme 2 The synthetic routes for **3a–d** and **4**.

prompted an investigation of the OPL performance in the solid state in polymer thin films.

Results and discussion

Synthesis and structural characterization

A TPE derivative bearing a hydrodisilyl substituent was prepared by lithiation of TPE-Br **1** with *n*-BuLi and subsequent reaction with 1 equiv. of 1,2-dichloro-1,1,2,2-tetramethyldisilane followed by *in situ* hydrogenation with $LiAlH_4$. The resulting product, **2**, is stable enough to be isolated by chromatography on silica gel and stored under ambient conditions for at least 6 months. TPE–Si–Si-D compounds **3a–d** were readily synthesized in reasonable yields by the Pd(0)-catalyzed coupling reactions of hydrodisilyl TPE **2** and the appropriate *para*-substituted iodobenzenes (Scheme 2).[11b,12c,17] Brief screening of reaction conditions were conducted to explore the best catalyst loading, base, solvent and temperature (Table S1, ESI†). TPE–Si–Si-A dyes with terminal electron-withdrawing substituents such as –COOEt, $–NO_2$, $–CF_3$, and –CHO were not obtained, however. This can probably be attributed to C–Si bond cleavage induced by the electron-withdrawing properties.[11b,18] A symmetric bis(disilyl)-bridged bisTPE compound, **4**, was also obtained by the same method using 1,4-diiodobenzene as a starting material. All the disilanyl bridged compounds were fully characterized by ^1H and ^{13}C NMR spectroscopy and high-resolution mass spectrometry. Thermal gravimetric analysis (TGA) revealed that all of the disilane-bridged molecules were highly thermally stable, with 5% weight loss over a range of 235–390 °C. The melting points of **3a–d** and **4** measured by differential scanning calorimetry (DSC) are 135, 148, 116, 130 and 196 °C, respectively (Fig. S1, ESI†).

Photophysical properties

The photophysical properties of **3a–d** and **4** were analyzed (Fig. 1 and Table 1) by measuring the UV-visible absorption spectra in solution along with emission spectra in both solution and the solid-state. Although bearing disilane bridges, these new compounds exhibit similar absorption spectral profiles to TPE (Fig. 1), resulting in exceptional optical transparency in the visible region (*ca.* 400–700 nm). The absorption band maxima of **3a–d** and **4** are red shifted by 6–8 nm relative to that of TPE due to σ–π conjugation between the Si–Si bond and the adjacent phenyl group. In the literature, 4-(1,2,2-triphenylvinyl)-1,10-biphenyl (TPE-Ph), in which TPE is directly connected with a phenyl group through π–π conjugation, exhibits a maximum absorption peak that is dramatically red shifted by 32 nm.[19] Thus, the Si–Si bridge affects the electronic structures more subtly than is the case with π-conjugated systems.

Published on 28 April 2021. Downloaded by Rhodes University on 11/3/2021 3:22:14 PM.

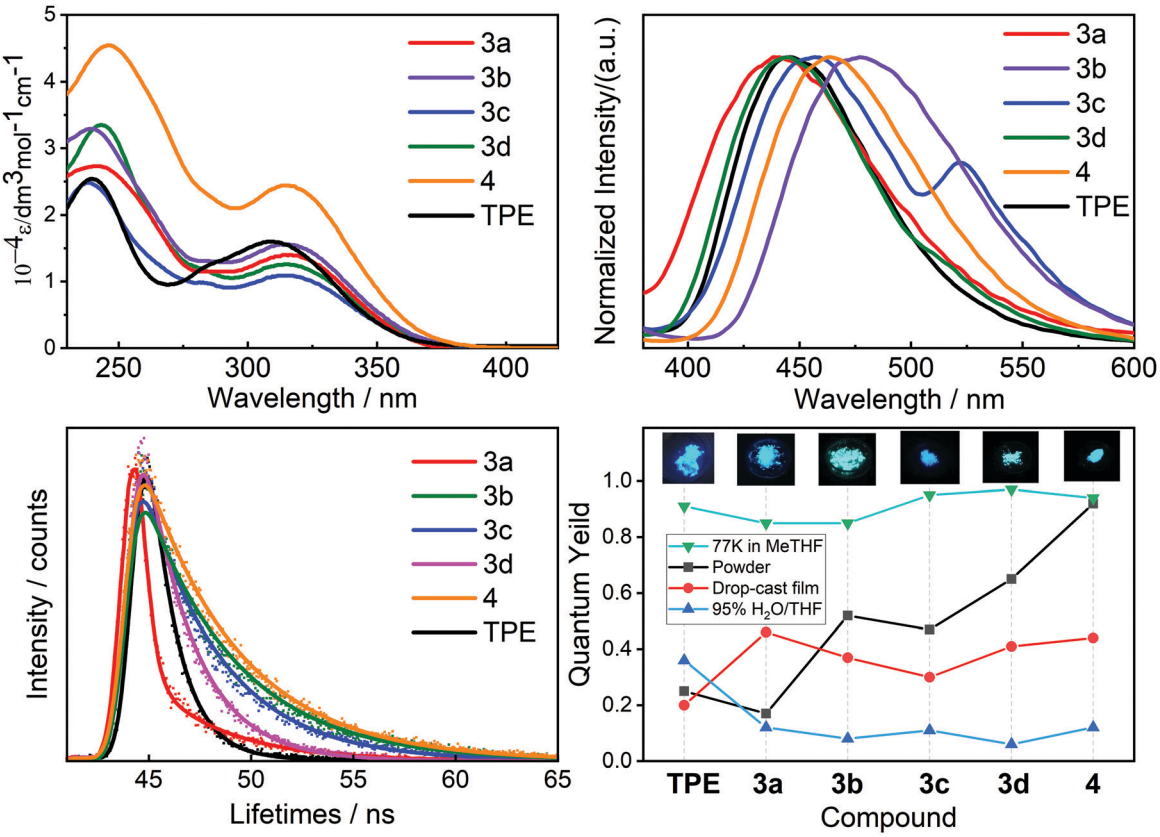

Fig. 1 (a) Absorption spectra of **3a–d**, **4** and **TPE** in THF solution. (b) Normalized PL spectra of powder samples (λ_{ex} = 360 nm). (c) Fluorescent lifetimes of **3a–d**, **4** and **TPE** in powder. (d) PL quantum yields under various conditions (inset pictures show the fluorescence color of the powder samples).

Table 1 Photophysical properties of TPE, **3a–d** and **4** in solution and the solid state

	UV	PL						
	THF	1 : 9 THF/H_2O (v/v)	Solid state					CIE(x, y)
	λ_{abs} (nm)	λ_{em} (nm)	$\lambda_{em}{}^a$ (nm)	QY^a (%)	τ^a (ns)	$k_r{}^b$ (10^8 s^{-1})	$k_{nr}{}^c$ (10^8 s^{-1})	Powder
TPE	308	464	450	25	1.33	1.88	5.64	(0.15, 0.08)
3a	314	482	438	17	1.90	0.89	4.37	(0.15, 0.08)
3b	315	478	477	52	3.80	1.37	1.26	(0.14, 0.17)
3c	315	478	457, 522	47	4.50	1.04	1.18	(0.15, 0.24)
3d	316	482	443	65	2.30	2.83	1.52	(0.15, 0.09)
4	316	475	462	92	4.60	2.00	0.17	(0.15, 0.15)

^{a} Absolute quantum yields measured in powder with an integration sphere. ^{b} The radiative decay rate in powder, k_r = QY/τ. ^{c} The nonradiative decay rate in solids, k_{nr} = (1 − QY)/τ.

It is noteworthy that the molar absorption coefficients for **4**, which has two TPE groups, are larger than those of TPE and **3a–d** (Fig. 1).

All the disilane-bridged compounds are non-fluorescent in organic solvents such as dichloromethane, THF, and CH_3CN. The aggregation-induced emission (AIE) effect was examined in THF/H_2O mixtures. As depicted in Fig. S2 (ESI†), all molecules exhibited very weak emission intensity when the water fraction (f_w) was <70%. The emission intensity increased markedly when f_w was >70%, and fluorescent aggregate particles were observed in the mixture, confirming their AIE properties. The emission maxima lie at 475–482 nm, red shifted by 11–18 nm compared with that of TPE. For **3a**, **3b**, **3d** and **4**, maximum emission intensity is observed when f_w reaches 99%. A rapid decrease in fluorescence intensity was observed for **3c** when f_w reached 99%, possibly due to a transition from the crystalline form to an amorphous state.[20]

The solid-state photoluminescence properties were also measured (Fig. 1 and Table 1). **3b** exhibits the same emission profile with almost the same emission maximum observed in powder and a 99% water/THF mixture. While **3a** and **3d** exhibit intense blue-shifted emission (44 and 39 nm), they have almost the same CIE(x,y) coordinates as TPE. The solid-state emission maxima of **4** and TPE are blue shifted by 13 and 14 nm relative to 99% water/THF solution, respectively. Obvious dual emission was observed for **3c** at 457 and 522 nm, which can be attributed to the unique packing mode in the powder state. **3d**

 This journal is © The Royal Society of Chemistry 2021

Published on 28 April 2021. Downloaded by Rhodes University on 11/3/2021 3:22:14 PM.

also exhibits a weak emission band at *ca.* 520 nm. The quantum yields of **3b**, **3c**, **3d** and **4** in powder are 1.9–3.7 times that of TPE. The bis-disilanyl bridged bis-TPE compound **4** possesses the highest quantum yield value of 0.92 in the context of powders, while its absorption and emission wavelength exhibit a red shift of only *ca.* 12 nm when compared with TPE. These results indicate that the Si–Si σ-bridge subtly modifies the spectral band, while the primary emission color of TPE is retained. The fluorescence lifetimes (τ) of **3b**, **3c**, **3d** and **4** exceed 2.30 ns, which is longer than those of TPE and **3a** (Fig. 1c and Table 1). The nonradiative decay rates (k_{nr}) obtained for **3b**, **3c**, **3d** and **4** are less than half those for TPE and **3a**, indicating that the enhanced emission efficiency is mainly facilitated by blocking nonradiative pathways. The fluorescence quantum yields of the disilanyl-bridged compounds are all larger than that of TPE in drop-cast films (0.30–0.46, Fig. 1d and Table S1, ESI†). When measured at 77 K in 2-methyltetrahydrofuran, the emission spectral profiles of **3a–d** and **4** are similar to that of TPE, with bands centered at 437 nm (Fig. S4, ESI†) and quantum yield values >85%.

Single crystal analysis

Single crystals of **3c** and **3d** were obtained by the slow diffusion of acetonitrile into CH_2Cl_2 solutions at room temperature. Detailed crystallographic data are summarized in Tables S3 and S4 (ESI†). Both crystals exhibit bright blue emission (Fig. S5, ESI†). The conformation of disilanes can vary significantly due to the flexibility of the disilane bridge. **3c** crystallizes in the chiral space group $P2_1$, and **3d** in the centrosymmetric space group $P2_1/c$. The torsion angles between the Si–Si σ-bonding axis and the phenyl ring plane primarily determine the degree of σ–π conjugation. It has been reported that orthogonal torsion angles favor the most effective σ–π conjugation.[21] In the structure of **3c**, the torsion angles are 65.87 and 84.21°, while those for **3d** are 73.98 and 68.39° (Fig. S6, ESI†), suggesting that the σ–π conjugation of **3c** is more effective. There are significant differences in the intermolecular interactions in these two crystals. In the structure of **3c**, multiple CH···π interactions between several molecules are observed with short contact distances (2.760–2.886 Å; Fig. 2c). This type of intermolecular interaction and the steric-hindrance effect of bulky Si atoms may work together to constrain the molecules in the crystal lattices and suppress the free rotations of the phenyl rings in the solid state. However, repulsive CH_3···PhH interactions (H···H distance: 2.351 Å; Fig. 2c)[14b] would have negative effects on the restriction of crystal packing. In the structure of **3d**, only CH···π interactions are formed between neighboring molecules with no H···H interactions observed. This suggests that it possesses a tighter crystal packing mode, which may explain its higher PL quantum yield in the solid state.

Theoretical investigation

The electronic structures of **3a–d** and **4** were explored theoretically through DFT and TD-DFT calculations performed at the B3LYP/6-31G(d) level of theory. TPE was also examined as a model compound. The geometries of **3c** and **3d** were optimized based on their crystal structures. Representative frontier molecular orbitals (MOs), their energies and the HOMO–LUMO gaps are summarized in Fig. 3. The LUMOs of all compounds are mainly localized on the TPE moiety, while the HOMOs are delocalized over the TPE moiety and the Si–Si σ-bond, suggesting the participation of Si–Si σ-electrons in the modulation of the electronic structures. In comparison with TPE, incorporating a disilane bridge stabilizes the LUMO energies (0.02–0.09 eV) but has a negligible impact on the HOMO energies. As a result, the HOMO–LUMO energy gaps of disilanyl-bridged compounds decrease slightly. This explains the slight band shifts observed in the absorption spectra. **3c** and **3d** have methoxy and phenoxy groups as the terminal groups, respectively. It is noteworthy that the electron density in the HOMO of **3c** spreads over the molecule across the Si–Si bridge and has significant MO coefficients on the phenyl group and the methoxy oxygen atom. In contrast, the electron density in the HOMO of **3d** exclusively localizes on the TPE moiety and the Si–Si σ-bond, which demonstrates that there is slightly inferior σ–π conjugation compared to **3c**.

OPL properties

The OPL properties of poly(bisphenol A carbonate) (PBC) thin films of **3a–d** and **4** were investigated at 532 nm by using the Z-scan method[22] with 7 ns laser pulses (35 μJ, 10 Hz) from a

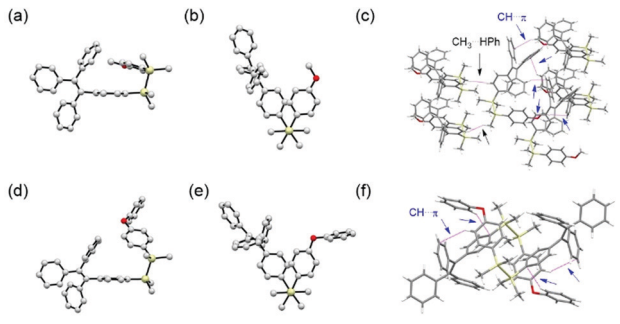

Fig. 2 Crystal structures of **3c** (top) and **3d** (bottom). (a) and (d) Side view. (b) and (e) Viewed along Si–Si bond. (c) and (f) Packing mode showing the CH···π (blue arrows) and CH_3–PhH contacts (black arrows). CCDC **3c**: 2061563 and **3d**: 2061564.†

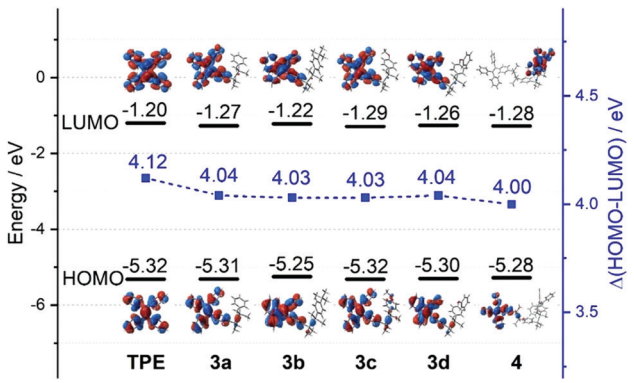

Fig. 3 Calculated energy levels and electronic density contours of the frontier π-MOs of TPE, **3a–d** and **4** at the B3LYP/6-31G(d) level of theory and an isosurface of 0.02 a.u.

Published on 28 April 2021. Downloaded by Rhodes University on 11/3/2021 3:22:14 PM.

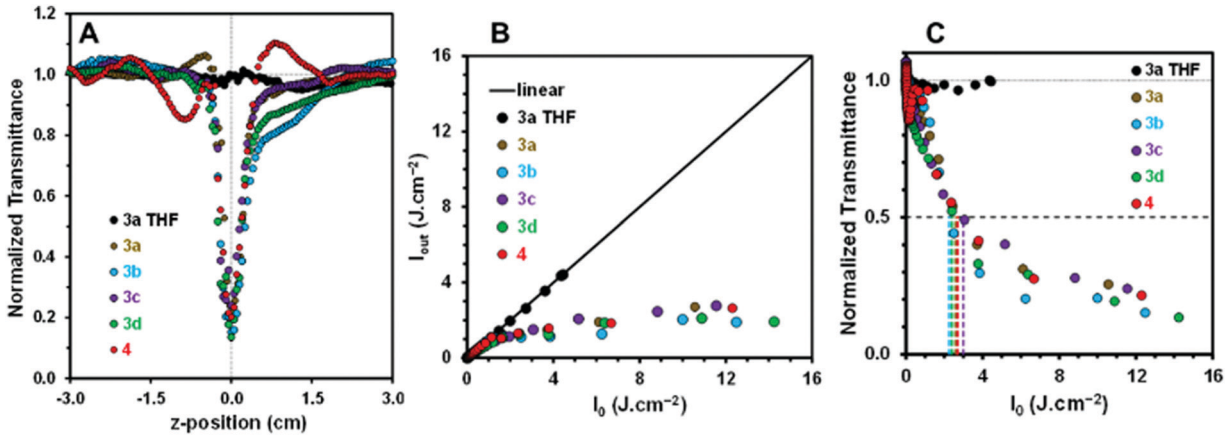

Fig. 4 (a) Z-scan data and (b) output fluence plots for the PBC polymer thin films of **3a–d** and **4**, and for **3a** in THF solution. (c) Calculation of the I_{lim} values for the PBC polymer thin films.

Spectra-Physics Quanta-Ray laser in a manner described previously.[5a] The transparent thin films were prepared using 9.0×10^{-5} M solutions (2.5 mL) in THF. PBC (100 mg) was added to the solutions, sonicated for 15 min and left to stir at room temperature. Using a drop and dry method, the solutions were transferred onto a glass slide placed on a Petri dish to form thin films. Film thicknesses of 8.5 ± 0.5 μm were measured using the knife-edge attachment of a Bruker D8 Discover X-ray diffraction (XRD) system. In the context of transparent PBC thin films, a strong reverse saturable absorbance (RSA) response was observed with normalized transmission decreased to around 0.2 at the laser focal point (Fig. 4(a)) with output fluence (I_{out}) reaching a plateau with increasing input fluence as anticipated for an optical power limiter (Fig. 4(b)). Since 7 ns laser pulses with a Gaussian laser pulse time profile were used,[5a] excited state absorption from the S_1 and/or T_1 states can contribute to the observed RSA response in addition to two-photon absorption that would dominate on a femtosecond timescale.[8] As a result, only effective nonlinear absorption coefficient (β_{eff}) values of 51, 110, 61, 91 and 48 cm GW^{-1} were obtained by fitting the RSA responses for the PBC polymer thin films of **3a–d** and **4**, respectively, using the equations reported by Sheik-Bahae[22] for the normalized transmittance of open aperture Z-scan measurements. The limiting threshold intensity (I_{lim}) is usually defined as the input fluence (I_0) value at which nonlinear transmittance is 50% lower than the linear transmittance value (Fig. 4(c)). I_{lim} values of 2.6, 2.3, 3.0, 2.4 and 2.7 J cm^{-2} were estimated for the PBC polymer thin films of **3a–d** and **4**, respectively. These values could be further lowered by increasing the concentration of dye used to prepare the thin films. In contrast, negligible OPL properties were observed in THF solution, and no significant RSA response was observed when a PBC thin film was prepared with TPE.

Conclusions

In summary, we report a series of readily synthesized disilanyl-bridged TPE derivatives. The presence of the Si–Si bridge can significantly enhance the solid-state emission efficiency up to 4 times while retaining a similar absorption band maximum and emission color to those observed in solution. The OPL performance of these novel σ-bridged molecules was examined in transparent PBC films by using the Z-scan method with 7 ns laser pulses (35 μJ) at 532 nm. Optical limiting thresholds of 2.3–3.0 J cm^{-2} were achieved that could be further enhanced by embedding a higher concentration of the dyes. The unique photophysical properties and excellent transparency in the visible region that result from the disilanyl-bridged architectures may open a new avenue for developing the next generation of OPL materials.

Experimental section

Materials and instruments

Reagents and solvents were purchased from commercial suppliers and used without further purification unless otherwise indicated. All air and moisture-sensitive reactions were carried out under an argon atmosphere in glassware that was dried in an oven at 120 °C and cooled under a stream of inert gas before use. Tetrahydrofuran was refluxed with sodium and distilled out immediately before use. ^{1}H NMR and ^{13}C NMR spectra were recorded on a Bruker DRX400 spectrometer and referenced to the residual proton signals of deuterated solvents ($CDCl_3$: 7.26 ppm; CD_2Cl_2: 5.32 ppm). HR-MS data were recorded on a Bruker Daltonics microTOF-Q II spectrometer. All solvents used for the spectroscopic measurements were of UV spectroscopic grade (Aldrich). Diffraction data were collected on a Bruker Smart Apex II CCD diffractometer or Bruker AXS Apex II diffractometer with graphite-monochromated Mo-Kα (λ = 0.71073 Å).

Synthesis and characterisation

Synthesis of hydrodisilyl TPE 2. (2-(4-Bromophenyl)ethene-1,1,2-triyl)tribenzene **1** (2 g, 5 mmol) was dissolved in dry ether under argon and cooled to −78 °C, *n*-BuLi (3.2 mL, 5 mmol, 1.6 M in hexane) was added dropwise. The mixture was stirred at −78 °C for 1.5 h and then quickly warmed to 0 °C. In another

 This journal is © The Royal Society of Chemistry 2021

Published on 28 April 2021. Downloaded by Rhodes University on 11/3/2021 3:22:14 PM.

flask, 1,2-dichlorotetramethyldisilane (1 mL, 5 mmol) was dissolved in dry ether (50 mL) under an argon atmosphere and cooled to −78 °C. The previous TPE–Li mixture was transferred into the flask and stirred for 2 h. The reaction mixture was gradually warmed up to room temperature, $LiAlH_4$ (189.5 mg, 5.0 mmol) was added, and the mixture was stirred overnight. The reaction was carefully quenched with water, and the aqueous layer was extracted three times with dichloromethane. The combined organic layer was washed with water and dried over sodium sulfate. The solvent was purified by chromatography over silica gel (9 : 1 petroleum ether/dichloromethane) to give compound **2** as a white powder (1.34 g, 60%).

^{1}H NMR (400 MHz, $CDCl_3$): δ 7.20 (d, J = 8 Hz, 2H), 7.11–7.07 (m, 9H), 7.05–6.98 (m, 8H), 3.70–3.64 (m, 1H), 0.33 (s, 6H), 0.06 (d, J = 4 Hz, 6H).

^{13}C NMR (100 MHz, $CDCl_3$): δ 143.79, 141.17, 137.01, 133.13, 131.49, 130.76, 127.76, 126.52, −3.59, −6.52 ppm.

Synthesis of 3a, 3b, 3c, and 3d. Under an argon atmosphere, compound **2** (449 mg, 1 mmol) and bis(tri-*tert*-butylphosphine) palladium(0) (15.3 mg, 0.03 mmol) were added to a solution of iodobenzene (111 μL, 1 mmol) in dry mesitylene (4 mL). *N*,*N*-Diisopropylethylamine (248 μL, 1.5 mmol) was added dropwise. The reaction mixture was stirred for 3 d at room temperature. The complete consumption of **2** was confirmed by TLC. The crude product was purified by chromatography over silica gel (1 : 10 DCM/petroleum ether) and recrystallized from pentane to afford **3a** at a yield of 36% (189 mg).

^{1}H NMR (400 MHz, $CDCl_3$): δ 7.23 (s, 4H), 7.08 (t, J = 6.8 Hz, 12H), 7.02–6.97 (m, 6H), 6.94 (d, J = 7.5 Hz, 2H), 0.24 (s, 6H), 0.22 (s, 6H).

^{13}C NMR (100 MHz, CD_2Cl_2): δ 144.16, 141.42, 139.40, 137.35, 134.24, 133.49, 131.58, 130.75, 128.69, 128.19–127.86, 126.75, 30.10, −3.94, −4.15.

HRMS-ESI: m/z: calcd $[C_{36}H_{36}Si_2 + Na]^+$ m/z = 547.2248, found m/z = 547.2245.

Compounds **3b**, **3c** and **3d** were obtained as white solid by using similar procedures to that for **3a** in yields of 32%, 36% and 30%, respectively.

3b: ^{1}H NMR (400 MHz, $CDCl_3$): δ 7.30 (d, J = 7.9 Hz, 2H), 7.23 (s, 1H), 7.10 (d, J = 1.8 Hz, 11H), 7.04 (d, J = 7.2 Hz, 7H), 6.97 (s, 2H), 1.32 (s, 9H), 0.27 (s, 6H), 0.23 (s, 6H).

^{13}C NMR (100 MHz, $CDCl_3$): δ 151.38, 143.88, 141.16, 137.15, 135.40, 133.90, 133.26, 131.49, 130.64, 127.74, 126.51, 124.74, 29.70, −3.51, −4.05.

HRMS-ESI: m/z: calcd $[C_{40}H_{44}Si_2 + Na]^+$ m/z = 603.2874, found m/z = 603.2864.

3c: ^{1}H NMR (400 MHz, $CDCl_3$): δ 7.21 (d, J = 8.5 Hz, 2H), 7.10 (t, J = 6.6 Hz, 11H), 7.03 (dd, J = 6.1, 3.5 Hz, 6H), 6.97 (d, J = 7.9 Hz, 2H), 6.85 (d, J = 8.4 Hz, 2H), 3.81 (s, 3H), 0.26 (s, 6H), 0.22 (s, 6H).

^{13}C NMR (100 MHz, CD_2Cl_2): δ 160.47, 144.16, 141.46, 137.54, 135.58, 133.50, 131.59, 130.71, 129.77, 127.99–127.97, 126.74, 113.74, 55.31, −3.72, −4.14.

HRMS-ESI: m/z: calcd $[C_{42}H_{40}OSi_2 + Na]^+$ m/z = 577.2353, found m/z = 577.2340.

3d: ^{1}H NMR (400 MHz, CD_2Cl_2): δ 7.37 (t, J = 7.8 Hz, 2H), 7.24 (d, J = 8.2 Hz, 2H), 7.10–7.00 (m, 20H), 6.96 (d, J = 7.8 Hz, 2H), 6.91 (d, J = 8.2 Hz, 2H), 0.28 (s, 6H), 0.25 (s, 6H).

^{13}C NMR (100 MHz, CD_2Cl_2): δ 158.06, 157.31, 144.24, 141.42, 135.79, 133.50, 131.57, 130.73, 130.15, 127.99, 126.75, 123.77, 119.47, 118.25, −3.81, −4.20.

HRMS-ESI: m/z: calcd $[C_{42}H_{40}OSi_2 + Na]^+$ m/z = 639.2510, found m/z = 639.2516.

Synthesis of 4. Compound **2** (898 mg, 2 mmol), 1,4-diiodobenzene (330 mg, 1 mmol) and bis(tri-*tert*-butylphosphine) palladium (0) (31 mg, 0.06 mmol) were dissolved in 4 mL dry mesitylene under argon. *N*,*N*-Diisopropylethylamine (496 μL, 3 mmol) was added dropwise to the solution at room temperature. The reaction mixture was stirred for 3 d at room temperature. The complete consumption of compound **2** was confirmed by TLC. The solution was removed under reduced pressure. The crude product was loaded onto a silica gel flash column (4 : 6 petroleum ether/dichloromethane) and recrystallized from pentane to afford product **4** as a white power (272 mg, 28%).

^{1}H NMR (400 MHz, CD_2Cl_2): δ 7.38 (t, J = 7.9 Hz, 2H), 7.22 (d, J = 8.4 Hz, 2H), 7.15–7.00 (m, 20H), 6.95 (d, J = 7.9 Hz, 2H), 6.90 (d, J = 8.3 Hz, 2H), 0.28 (s, 6H), 0.26 (s, 6H).

^{13}C NMR (100 MHz, $CDCl_3$): δ 144.00–143.65, 141.15, 136.96, 133.18, 131.49, 130.64, 127.74, 126.53, 38.29, 31.39, 29.86, −4.09.

HRMS-ESI: m/z: calcd $[C_{66}H_{66}Si_4 + K]^+$ m/z = 1009.3873, found m/z = 1009.3864.

Spectroscopic measurements

UV-visible absorption spectra were recorded on a Shimadzu 1800 spectrophotometer. Fluorescence spectra and the fluorescence lifetimes of the samples were determined with a Horiba Jobin Yvon Fluorolog-3 spectrofluorimeter. The goodness of the fits of the single exponential decays were assessed by using chi-squared (χ_R^2) and autocorrelation function $C(j)$ values. Low residuals ($\chi_R^2 < 1.2$) were consistently observed. For samples in solution, absorption and emission measurements were carried out in 1 × 1 cm quartz cuvettes. The absolute quantum yields (Φ_F) and emission spectra in the solid state were measured on Horiba Jobin Yvon Fluorolog-3 spectrofluorimeter with an integrating sphere. For all measurements, the temperature was kept constant at (298 ± 2) K. When the fluorescence decays were monoexponential, the rate constants of radiative (k_r) and nonradiative (k_{nr}) deactivation were calculated from the measured fluorescence quantum yield and fluorescence lifetime (τ) according to eqn (1) and (2):

$$k_r = \Phi_F/\tau \quad (1)$$

$$k_{nr} = (1 - \Phi_F)/\tau \quad (2)$$

DFT calculations

The G09W software package was used to carry out a DFT geometry optimization using the B3LYP functional with 6-31G(d) basis sets.[23] UV-visible spectra were calculated by using the time-dependent density functional theory (TD-DFT) approach with the B3LYP functional and 6-31G(d) basis sets.

Published on 28 April 2021. Downloaded by Rhodes University on 11/3/2021 3:22:14 PM.

Conflicts of interest

There are no conflicts to declare.

Acknowledgements

This work was supported by the National Natural Science Foundation of China (Fund No. 21871072 and 21801057) to HL, and the National Research Foundation (NRF) of South Africa ISRR grant (uid: 119259) to JM, and the Department of Science and Technology (DST) Nanotechnology (NIC)/NRF of South Africa through DST/NRF South African Research Chairs Initiative to Professor of Medicinal Chemistry and Nanotechnology (uid: 62620) to TN.

Notes and references

1 S. D. Smith, *Nature*, 1985, **316**, 319–324.
2 C. W. Spangler, *J. Mater. Chem.*, 1999, **9**, 2013–2020.
3 M. Pawlicki, H. A. Collins, R. G. Denning and H. L. Anderson, *Angew. Chem., Int. Ed.*, 2009, **48**, 3244–3266.
4 L. W. Tutt and A. Kost, *Nature*, 1992, **356**, 225–226.
5 (*a*) N. Ndebele, Z. Hlatshwayo, B. P. Ngoy, G. Kubheka, J. Mack and T. Nyokong, *J. Porphyrins Phthalocyanines*, 2019, **23**, 701–717; (*b*) G. Kubheka, O. Achadu, J. Mack and T. Nyokong, *New J. Chem.*, 2017, **41**, 12319–12325.
6 M. O. Senge, M. Fazekas, E. G. A. Notaras, W. J. Blau, M. Zawadzka, O. B. Locos and E. M. Ni Mhuircheartaigh, *Adv. Mater.*, 2007, **19**, 2737–2774.
7 (*a*) Y. Chen, M. Hanack, Y. Araki and O. Ito, *Chem. Soc. Rev.*, 2005, **34**, 517–529; (*b*) Y. Chen, S. O'Flaherty, M. Fujitsuka, M. Hanack, L. R. Subramanian, O. Ito and W. J. Blau, *Chem. Mater.*, 2002, **14**, 5163–5168; (*c*) M. Sebastian, A. Ganesan, H. Behbehani, A. Husain and S. Makhseed, *J. Phys. Chem. C*, 2020, **124**, 21740–21750.
8 D. Dini, M. J. F. Calvete and M. Hanack, *Chem. Rev.*, 2016, **116**, 13043–13233.
9 R. Misra and S. P. Bhattacharyya, *Intramolecular Charge Transfer – Theory and Applications*, Nonlinear Optical Response of ICT Molecules, Wiley-VCH, 2018, ch. 5, pp. 149–195, DOI: 10.1002/9783527801916.ch5.
10 G.-J. Zhou, W.-Y. Wong, Z. Lin and C. Ye, *Angew. Chem., Int. Ed.*, 2006, **45**, 6189–6193.
11 (*a*) T.-C. Lin, Y.-H. Lee, B.-R. Huang, M.-Y. Tsai and J.-Y. Lin, *Dyes Pigm.*, 2016, **134**, 325–333; (*b*) X. Zheng, W. Du, L. Gai, X. Xiao, Z. Li, L. Xu, Y. Tian, M. Kira and H. Lu, *Chem. Commun.*, 2018, **54**, 8834–8837.
12 (*a*) S. Hirata, M. Nishio, H. Uchida, T. Usuki, T. Nakae, M. Miyachi, Y. Yamanoi and H. Nishihara, *J. Phys. Chem. C*, 2020, **124**, 3277–3286; (*b*) T. Usuki, M. Shimada, Y. Yamanoi, T. Ohto, H. Tada, H. Kasai, E. Nishibori and H. Nishihara, *ACS Appl. Mater. Interfaces*, 2018, **10**, 12164–12172; (*c*) S. Wang, H. Lu, Y. Wu, X. Xiao, Z. Li, M. Kira and Z. Shen, *Chem. – Asian J.*, 2017, **12**, 561–567; (*d*) S. Feng, Z. Zhou, X. Xiang, H. Feng, Z. Qu and H. Lu, *ACS Omega*, 2020, **5**, 19181–19186.
13 E. A. Marro and R. S. Klausen, *Chem. Mater.*, 2019, **31**, 2202–2211.
14 (*a*) X. Xiang, Z. Zhou, H. Feng, S. Feng, L. Gai, H. Lu and Z. Guo, *CCS Chem.*, 2020, **2**, 329–336; (*b*) M. Nishio, M. Shimada, K. Omoto, T. Nakae, H. Maeda, M. Miyachi, Y. Yamanoi, E. Nishibori, N. Nakayama, H. Goto, T. Matsushita, T. Kondo, M. Hattori, K. Jimura, S. Hayashi and H. Nishihara, *J. Phys. Chem. C*, 2020, **124**, 17450–17458; (*c*) M. Shimada, Y. Yamanoi, T. Ohto, S.-T. Pham, R. Yamada, H. Tada, K. Omoto, S. Tashiro, M. Shionoya, M. Hattori, K. Jimura, S. Hayashi, H. Koike, M. Iwamura, K. Nozaki and H. Nishihara, *J. Am. Chem. Soc.*, 2017, **139**, 11214–11221.
15 (*a*) G. Mignani, A. Kramer, G. Puccetti, I. Ledoux, G. Soula, J. Zyss and R. Meyrueix, *Organometallics*, 1990, **9**, 2640–2643; (*b*) J. J. Tan and F. L. Gu, *ChemistrySelect*, 2018, **3**, 10244–10249.
16 (*a*) J. Mei, N. L. C. Leung, R. T. K. Kwok, J. W. Y. Lam and B. Z. Tang, *Chem. Rev.*, 2015, **115**, 11718–11940; (*b*) J. Yang, Z. Chi, W. Zhu, B. Z. Tang and Z. Li, *Sci. China: Chem.*, 2019, **62**, 1090–1098; (*c*) Y.-J. Jin, H. Kim, J. J. Kim, N. H. Heo, J. W. Shin, M. Teraguchi, T. Kaneko, T. Aoki and G. Kwak, *Cryst. Growth Des.*, 2016, **16**, 2804–2809; (*d*) J. Xiong, X. Li, C. Yuan, S. Semin, Z. Yao, J. Xu, T. Rasing and X.-H. Bu, *Mater. Chem. Front.*, 2018, **2**, 2263–2271.
17 (*a*) L. Chen, J.-B. Huang, Z. Xu, Z.-J. Zheng, K.-F. Yang, Y.-M. Cui, J. Cao and L.-W. Xu, *RSC Adv.*, 2016, **6**, 67113–67117; (*b*) M. Shimada, Y. Yamanoi, T. Matsushita, T. Kondo, E. Nishibori, A. Hatakeyama, K. Sugimoto and H. Nishihara, *J. Am. Chem. Soc.*, 2015, **137**, 1024–1027.
18 C. Eaborn, *J. Organomet. Chem.*, 1975, **100**, 43–57.
19 H. Wang, Y. Li, Y. Zhang, J. Mei and J. Su, *Chem. Commun.*, 2019, **55**, 1879–1882.
20 X. Luo, J. Li, C. Li, L. Heng, Y. Q. Dong, Z. Liu, Z. Bo and B. Z. Tang, *Adv. Mater.*, 2011, **23**, 3261–3265.
21 M. Kira, T. Miyazawa, H. Sugiyama, M. Yamaguchi and H. Sakurai, *J. Am. Chem. Soc.*, 1993, **115**, 3116–3124.
22 (*a*) M. Sheik-Bahae, A. A. Said, T. Wei, D. J. Hagan and E. W. V. Stryland, *IEEE J. Quantum Electron.*, 1990, **26**, 760–769; (*b*) M. Sheik-bahae, A. A. Said and E. W. Van Stryland, *Opt. Lett.*, 1989, **14**, 955–957.
23 M. J. Frisch, G. W. Trucks, H. B. Schlegel, G. E. Scuseria, M. A. Robb, J. R. Cheeseman, G. Scalmani, V. Barone, B. Mennucci, G. A. Petersson, H. Nakatsuji, M. Caricato, X. Li, H. P. Hratchian, A. F. Izmaylov, J. Bloino, G. Zheng, J. L. Sonnenberg, M. Hada, M. Ehara, K. Toyota, R. Fukuda, J. Hasegawa, M. Ishida, T. Nakajima, Y. Honda, O. Kitao, H. Nakai, T. Vreven, J. A. Montgomery Jr, J. E. Peralta, F. Ogliaro, M. Bearpark, J. J. Heyd, E. Brothers, K. N. Kudin, V. N. Staroverov, R. Kobayashi, J. Normand, K. Raghavachari, A. Rendell, J. C. Burant, S. S. Iyengar, J. Tomasi, M. Cossi, N. Rega, J. M. Millam, M. Klene, J. E. Knox, J. B. Cross, V. Bakken, C. Adamo, J. Jaramillo, R. Gomperts, R. E. Stratmann, O. Yazyev, A. J. Austin, R. Cammi, C. Pomelli, J. W. Ochterski, R. L. Martin, K. Morokuma, V. G. Zakrzewski, G. A. Voth, P. Salvador, J. J. Dannenberg, S. Dapprich, A. D. Daniels, Ö. Farkas, J. B. Foresman, J. V. Ortiz, J. Cioslowski and D. J. Fox, *Gaussian 09, Revision A.1*, Gaussian, Inc., Wallingford CT, 2009.

 This journal is © The Royal Society of Chemistry 2021